Mode I Fatigue Crack Growth Behaviour in a Welded Cruciform Joint under Biaxial Stresses

Xiang Zhang[1,*], Haiying Zhang[2], Rui Bao[3]

[1] Department of Aerospace Engineering, School of Engineering, Cranfield University, Bedford, MK43 0AL, UK
[2] Aircraft Strength Research Institute, Xi'an, 710065, P.R. China
[3] Institute of Solid Mechanics, School of Aeronautic Science & Engineering, Beihang University, Beijing, 100191, P.R. China

* Corresponding author: xiang.zhang@cranfield.ac.uk

Abstract Biaxial load fatigue crack growth tests were performed for a cruciform joint made of aluminium-lithium alloy 2198-T8 containing a butt weld joint fabricated by the friction stir welding process. In all tests crack propagated in parallel with the weld joint. Two material rolling directions were studied in relation to the welding and crack growth direction, showing that the material rolling direction affects the crack growth path. Specimens welded orthogonally to the rolling direction exhibit shorter fatigue life than specimens welded parallel to the rolling direction. A simple method is then developed for predicting crack growth rate. FEM is used to calculate the stress intensity factors and *T* stress, which are subsequently used to predict the crack propagation rates and trajectory. Influence of applied stress biaxiality on stress intensity factors, *T* stress, crack trajectory and growth rates have been analysed. Out-of-plane bending caused by the specimen geometry is also modelled. Predicted and test measured crack growth lives are in reasonably good agreement. Reasons for discrepancy are discussed.

Keywords: Biaxial stresses, weld joint, crack propagation, fatigue, finite element method, aluminium alloy

1. Introduction

Trend in aircraft structural design and manufacture has been moving towards more integral structures by extrusion, machining and welding rather than the traditional mechanical fastening. Fatigue crack growth behaviour under biaxial stresses is complex even without weld joints. Welding will add additional challenge in the analysis due to the process induced residual stress and changes in weld metal microstructure and mechanical properties.

Fatigue crack growth behaviour in aluminium welded joints has been investigated by experiments [e.g. 1-2], analysis [3], or modelling [4-7]. These research efforts were carried out under the uniaxial load cases. Current state-of-the-art in predicting crack growth rates is to use empirical crack growth laws and incorporate the effective stress intensity factor ratio.

Biaxial load fatigue crack growth behaviour (without weld) has been investigated [8-16] for various applied biaxial load ratios ($k = \sigma_y/\sigma_x$). In summary, qualitatively similar results have been reported for a number of steel and aluminium alloys that crack growth rate is higher at k=-1 (pure shear), than k=0 (uniaxial) followed by k=1. Difference in the growth rates in different biaxial stress ratios depends also on the magnitude of applied stress. In terms of crack growth trajectory, crack was kept straight at $k \leqslant 1$ [10-11]. Crack growth deviation was found to be dependent on the K_I/T ratio [13-15]. The maximum tangential stress criterion (function of K_I and K_{II}) is widely used for crack turning analysis [17]. The criterion is implemented in some FE codes, e.g. ABAQUS and FRANC2D/3D.

The influence of weld joint (in terms of welding residual stress and microstructure change) on crack

growth behaviour and their interaction with the applied biaxial loads should be investigated. With this motivation, experimental test was conducted on a cruciform specimen made of aluminium alloy 2198-T8 containing a butt weld joint and subject to biaxial loads [18], which is briefly summarised in Section 2. This paper focuses on the modelling of crack growth behaviour.

2. Summary of fatigue tests

Four cruciform specimens were manufactured and tested under biaxial stresses [18]. Geometry and dimensions are shown in Fig. 1. The specimens were made of aluminium-lithium alloy 2198-T8 and joined by the friction stir weld (FSW) process. The panel skin has nominal thickness of 1.6 mm and the weld area has a nominal thickness of 3.1 mm. The top side of the thicker pad-up area measures 50 mm wide and the bottom side (specimen flat surface) is about 62 mm wide, making the average width of the pad-up 56 mm. Specimen COI-BIAX1 and COI-BIAX3 had weld seam orthogonal to the material rolling direction, whereas the weld path in COI-BIAX2 and COI-BIAX4 was parallel to the rolling direction. Initial crack was introduced parallel to the weld seam orientation and located at the specimen geometric centre. It is in the thermal-mechanical affected zone (TMAZ) on the so-called weld retreating side, about 5 mm from the weld nugget centre. The weld centre is not placed in the specimen geometric centre. Details are in Table 1. All tests were performed at applied biaxial stress ratio k = 1 and maximum nominal stress 100 MPa acting on the 250-mm-wide loading arm area with the thickness of 1.6 mm. The cyclic stress ratio was 0.1 in both load directions. Details of test measured crack growth lives and growth path can be found in [18]. Test results are presented in Section 4 in comparison with predicted crack growth behaviour. Further studies were undertaken by performing numerical modelling on various k ratios (k=0-2) to investigate the influence of biaxial stress ratio on crack growth rate and trajectory.

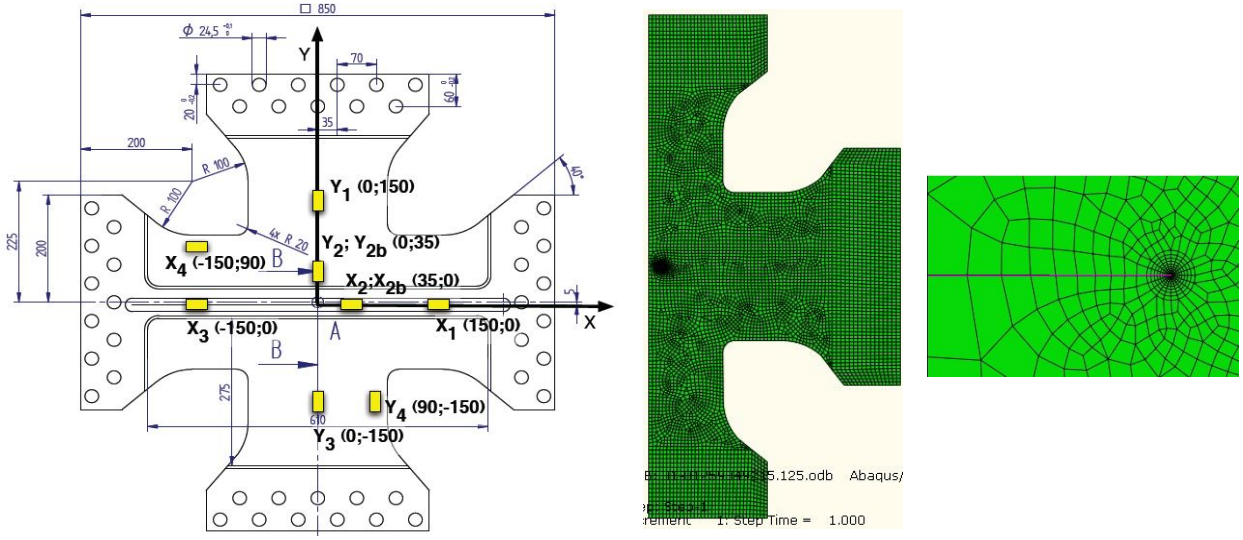

Fig 1. a) Test specimen and strain gauge locations (thickness of pad-up and griping area is 2.8 mm; skin pocket thickness is 1.6 mm); b) FE model of ½ specimen and local model of the crack tip.

Table 1 Test specimens and loading condition (applied stress σ_y = 40 kN)

Specimen No.	Weld orientation	Applied load ratio (k)
COI-BIAX1	Weld orthogonal to rolling direction	1
COI-BIAX2	Weld parallel to rolling direction	1
COI-BIAX3	Weld orthogonal to rolling direction	1
COI-BIAX4	Weld parallel to rolling direction	1

3. Computational analysis

3.1. FE model

Commercial code ABAQUS [19] was used. One half of the specimen was modelled using the second-order 8-node quadrilateral shell element. All elements are offset to the back surface (flat surface) to model the thickness variation in the pad-up and clamping areas. Due to the thickness change in the pad-up and four load-end clamping areas, there is considerable out-of-plane bending deformation even the panel is subjected to in-plane tensile load. This secondary bending can cause variation in the stress intensity factors (SIF). Therefore, prior to performing the fracture mechanics analysis, crack-free specimen was modelled first to verify the FE model against the strain gauge measurement at locations indicated in Fig. 1a. To model the secondary bending more accurately, 3D solid elements were used to provide a benchmark solution to the subsequent shell element models. In order to capture the bending deformation more accurately four elements are used through the 1.6 mm thickness. Out-of-plane deformation and strains were also calculated by the shell element model. Calculated strains and deformation agree with the 3D model output. Model geometry detail is given in Table 2.

Table 2 Configurations in FE models (unit: mm)

Configuration	a_o	h	t_1	t_2
1	10	30	2.80	1.60
2	20	56	3.11	1.55

Note: Configuration 1 is for numerical model only; Configuration 2 has the same dimension as the test specimen; a_o is half initial crack length, h is the pad-up width; t_1, t_2 are the pad-up and skin pocket thickness, respectively.

3.2. Fracture mechanics analysis

SIF is calculated using the interaction integral method available in the ABAQUS, which is similar to the *J*-integral method. FE model with an initial crack is shown in Fig. 1b. The middle nodes of the rosette elements around the crack tip are moved to the quarter-point position in order to model the crack tip stress singularity more accurately. User can instruct the ABAQUS code to extract the K_I, K_{II} and *T*-stress for each given crack length using the integration integral technique and then predict the crack propagation trajectory using the maximum tangential stress criterion. Subsequent crack configuration will be implemented by the user to manually extend the crack tip in the predicted direction by a specified crack extension increment. Subsequently, the area around the crack path will be re-meshed and the calculation of the SIF and crack growth angle repeated until a user-defined or critical crack length is reached. Calculated SIF (K_I) is normalised by the crack length and applied stress perpendicular to the crack plane, σ_y, to find the β factor:

$$\beta = \frac{K_I}{\sigma_y \sqrt{\pi a}} \qquad (1)$$

The β vs. a relation is then used in conjunction with the measured weld metal da/dN vs. ΔK data for life prediction. For variable amplitude loading with the same biaxial load ratio (k), ΔK for a specific load cycle can be found by multiply β by the applied stress range perpendicular to the crack growth path ($\Delta\sigma_y$). Weld metal crack growth rate (da/dN vs. ΔK) was measured under uniaxial-load [20] using “middle crack tension” geometry specimen, M(T), made of the same alloy and same welding

process. The weld was perpendicular to the applied load direction. Hence, the weld metal microstructure should be the same as that of the cruciform. Crack growth rates in the M(T) were obtained from constant amplitude load tests at R = 0.1.

4. Results and Discussion

4.1 Deformation, strain and stress

Due to the secondary bending effect the panel exhibits out-of-plane deformation even the load is in-plane. Calculated stress contours show a double curvature shaped deformation Fig 2. Positive deformation on the face of the pad-up side means bending towards the pad-up side. The maximum out-of-plane displacement is just outside the pad-up area with a value of 2.5 mm (k = 0) and 2.2 mm (k = 1). The panel centre (where the crack growth path is) is also bending towards the pad-up side with smaller displacement of 1.8 mm (k = 0) and 1.5 mm (k = 1). The bending deformation shown in Fig 2 is under the applied load of 40 kN (equal to a stress of 100 MPa in the loading arm of 1.6 mm thickness). The FE model shows that bending magnitude depends on the applied stress as well as the biaxial stress ratio. Under the same y-axis applied load, uniaxial loading results in more out-of-plane deformation (k = 0, Fig. 2a) than that by equal-biaxial case (k = 1, Fig. 2b), but the bending pattern is the same and the difference in bending magnitude is small. The out-of-plane deformation and in-plane strains were calculated using both 3D solid elements and 2D shell element; calculated values agree with each other. Therefore the thin-shell elements are employed in the crack growth models to reduce the computational cost. Computed strains agree well with the measured at most of the strain gauge positions, and the computed deformation pattern agrees with that described by the distributions of the strain gauges.

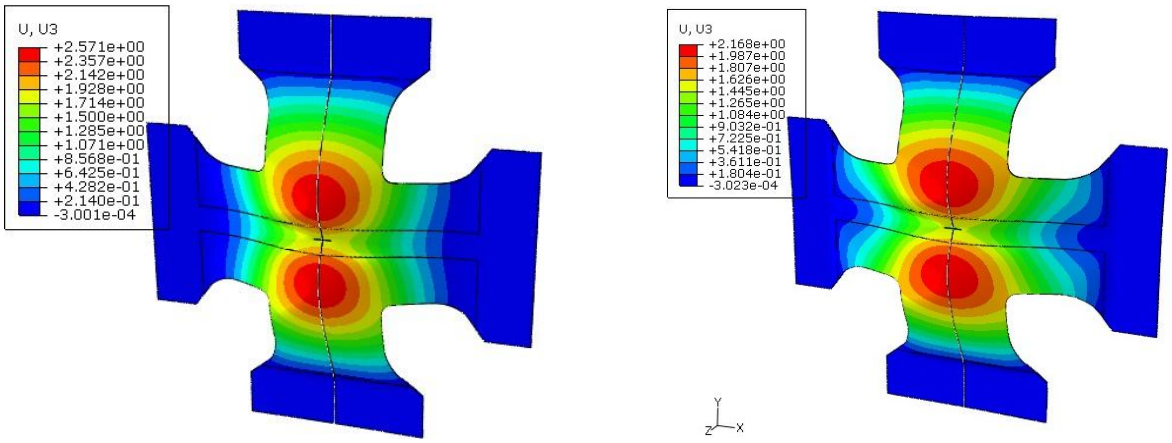

Fig. 2 Calculated out-of-plane deformation by 3D FE model under applied stress 100 MPa (figure showing the pad-up face): a) uniaxial load (k = 0); b) biaxial load (k = 1)

4.2 Stress intensity factors

Four biaxial load ratios (k = 0, 0.5, 1, 2) were modelled at the applied stress σ_y=100 MPa acting on the loading arm of the cross section of 250 mm width x 1.6 mm thickness. This stress level is reduced in the wider section and will be further reduced at the thicker pad-up area where the crack propagates. Calculated σ_y in the pad-up area is about 50 MPa [21]. Cases were also modelled for k = 1, 2 at applied stress σ_y = 50 MPa. Calculated mode I stress intensity factors (K_I) at the different k

are presented in Fig. 3a. As the k increases, K_I will decrease. Since crack growth rate is an exponential function of ΔK and the Paris law exponent is usually 2-4 for aluminium alloys, crack growth rate will be significantly reduced as the biaxial load ratio increases. This is reported in test measured crack growth rates [11-12]. Fig. 3b shows the non-dimensional K, i.e. the β factor by eq. (1), which is independent of the y-axis applied stress σ_y.

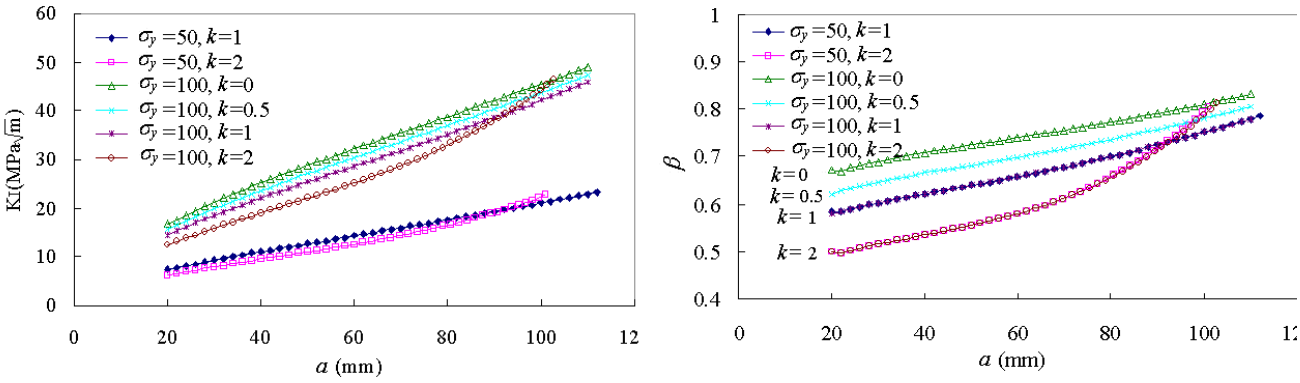

Fig. 3 FE calculated stress intensity factors under various biaxial load ratios: a) K_I; b) β factor.

4.3 Prediction of crack growth life and trajectory

Fig 4 shows comparison of predicted and test measured crack growth lives. There are three possible reasons for underestimating the crack growth life. 1) Residual stress effect was accounted for by using the measured *da*/*dN* data of an M(T) specimen fabricated by the same welding process with crack growing parallel in weld (perpendicular to the load direction) [20]. The magnitude of residual stresses are not exactly the same due to different geometry and size between the M(T) and cruciform specimens. However, since the welds were parallel to the crack growth path in both specimens, the transverse residual stress, which is perpendicular to the crack plane, is low in magnitude compared to the longitudinal residual stress parallel to the crack plane. Therefore the effect of transverse residual stress on crack growth is considered to be small. 2) Influence of weld metal microstructure change on crack growth rates is also contained in the measured *da/dN* data from the M(T). However, crack in the M(T) had was in the weld nugget centre, but the cruciform specimens had weld in the weld TMAZ zone about 5 mm from the weld nugget centre. Microstructures in these two zones are different, and this difference in microstructure is not modelled in this work. 3) FE calculated y-axis strains are found to be higher than the test measurement, leading to higher SIF values and, consequently, shorter predicted crack growth life.

Fig. 4b shows the measured and predicted crack growth trajectories. Calculated crack trajectory is modelled by crack extension under static loading rather than cyclic loading. Crack turning is predicted by the maximum tangential stress criterion in the Abaqus code. Calculated maximum crack deviation for “Configure 1” is about 3 mm, which is larger than that of “Configuration 2 (test specimen geometry)”. The difference is caused by the width of the pad-up, which is 30 mm and 56 mm, respectively. Narrower pad-up (30 mm) encourages crack deviation into the thinner skin. Although crack turning is predicted by the FE modelling, calculated crack deviation magnitude is smaller than the test measured Fig. 4b. Predicted deviation also started at longer crack length (120

mm) comparing to the test results [18].

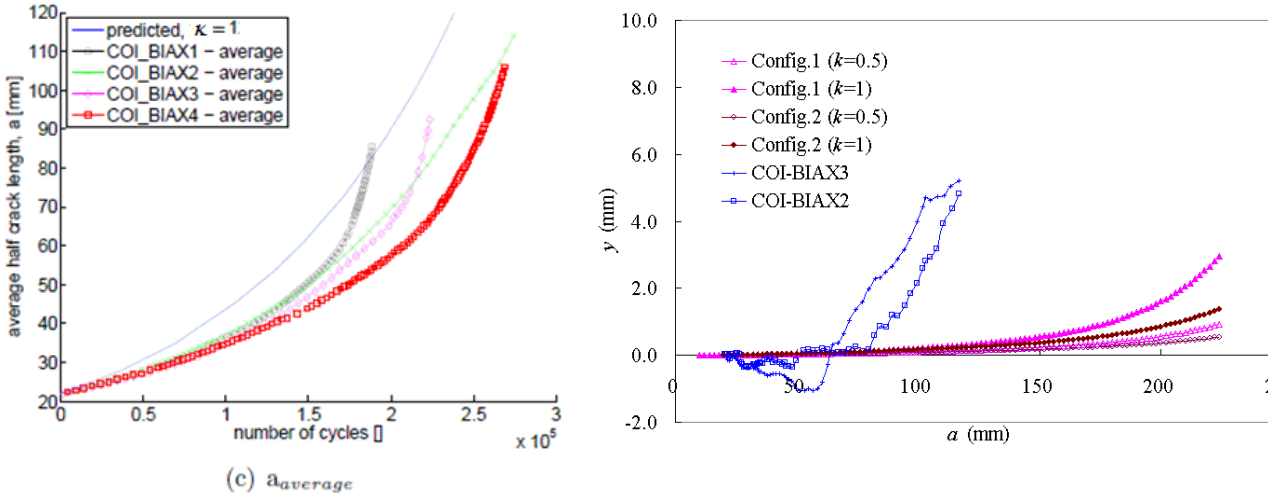

Figure 4 a) predicted crack growth life and b) trajectory, and comparison with test measurement.

4.4 Discussion based on further FE analysis

4.4.1. Influence of biaxial stress ration on crack growth rate

Mode II SIF (K_{II}) was calculated using the Abaqus interactive integration method [19]. Model shows that K_{II} is virtually zero for k = 0, 0.5 & 1. For k = 2 and at longer crack lengths (a > 60 mm), K_{II} has very low values of 0.3-0.6 MPa√m [21]. Since all specimens were tested at k = 1, K_{II} influence can be neglected. According to the literature, influence of lateral stress σ_x on crack growth rates is negligible in aluminium sheets [10] and steel alloys [11] under constant amplitude loading, if biaxial load ratio (k) is within the range of -1.5 to 1.75. Note work reported in [10-11] was for plain metals (no welds). In the test measured crack growth and life prediction analysis presented in Fig. 4, changes in weld metal properties and weld residual stresses are accounted for by using the weld metal property of da/dN vs. ΔK data.

4.4.2. Influence of biaxial stress on crack trajectory

It has been shown that applied mixed mode loading is the main cause of a major loss of directional stability [14]. Apart from K_{II}, the elastic T-stress (a stress quantity parallel to the crack face) is also a useful quantity for assessing the crack stability and kinking for linear elastic materials. T-stress is directly proportional to the load applied to the cracked part and also depends on its geometry. It has been shown that for small amount of crack growth under the mode I loading, a straight crack path will be stable when T < 0, whereas the path will be unstable when T > 0 [22]. In this paper T-stress is calculated by the Abaqus code. Fig 5 shows calculated T-stress normalised by the applied stress; positive values indicate the likelihood of crack deviation. For the test case of k = 1, T-stress is about the same magnitude of the applied stress when half crack length is beyond 40 mm. However, it is also reported that some cracks are directionally stable when T > 0 [15].

To explain the observed crack turning (Fig. 4b), we use the T_R parameter as defined in Eq. (2) [23]:

$$T_R = \frac{T}{\sigma_x} \qquad (2)$$

where $\sigma_x = K_I/\sqrt{(2\pi r)}$ is the crack tip *local* stress component parallel to the crack plane and r is the distance to the crack tip. Pook [23] recommends that T_R is evaluated at a characteristic distance $r = r_{ch}$, which is the same order of a microstructural feature size. Taking r_{ch} = 0.0159 mm [23], using Eq. (2) and the MN-m units, find:

$$T_R = 0.01\frac{T}{K_I} \qquad (3)$$

According to [15, 23], when T_R exceeds its critical value T_{RC}, crack will deviate from its original path. In [15] Pook stated a typical T_{RC} value suitable for many metals as at least 0.021 (unit: $m^{-1/2}$).

Calculated T_R values for various k ratios are presented in Fig. 6. For the test case of k =1, at half crack length a = 50 mm, calculated T_R according to Eq. (3) is 0.038 $m^{-1/2}$, which is greater than the suggested T_{RC} value. Therefore, under *tension* biaxial loading at ratio k=1, calculated crack deviation was expected, however the magnitude of deviation is small, just 3 mm away from the original crack path (Fig. 4b), which is not a major loss of directional stability. Measured crack deviation was nearly doubled at 5 mm, and crack deviation started at much earlier in shorter crack length (Fig. 4b). This discrepancy could be due to the changes in weld metal microstructure and the anisotropy property of the 2198-T8 alloy as reported in [24-25]. Material microstructure change and anisotropy properties were not modelled in this study.

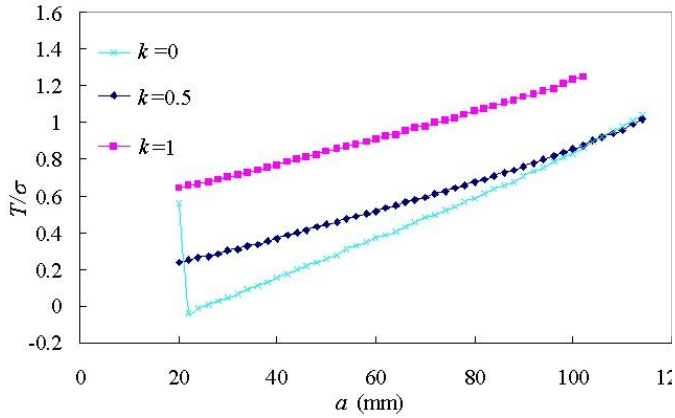

Fig. 5 T-stress (normalised by applied stress σ_y).

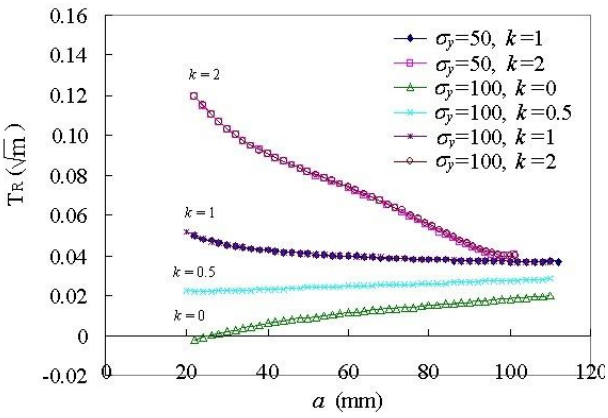

Fig. 6 Calculated T_R distribution.

4.4.3. Influence of weld-induced residual stress

Test measured crack turning is more pronounced than FEA predicted, Fig. 4b. One possible reason could be that the longitudinal residual stresses were present in the test specimen making the *actual* biaxial load ratio much higher than 1, but this residual stress was not considered in the prediction model. In this work, K_I, K_{II} and T are calculated for biaxial load ratio k = 1 without considering the welding-induced residual stresses. If the longitudinal residual stress (e.g. 150 MPa maximum magnitude according literature) is added to the applied lateral stress σ_x, then the biaxial stress ratio k

is about 2.5. According to the literature, no crack turning was observed at k = 0, 0.5 and 1 [11], but crack will turn when k > 2 [10]. Therefore there is more crack deviation in the test than predicted.

We have used the weld metal *da/dN* data for the life prediction presented in Fig. 4a, in which residual stress effect is included in the coupon tests to acquire the *da*/*dN* data. However, we have not used the combined lateral stresses ($\sigma_{x\_applied} + \sigma_{x\_residual}$) in the calculation of the crack growth driving forces (K_I, K_{II}, and T-stress); this could affect the magnitude of crack turning. Further, although residual stress effect is reflected in the measured crack growth data of welded M(T) sample with a same transverse weld, because the cruciform specimen has different geometry and dimension, welding induced residual stresses in the cruciform specimen could be different from those in the M(T).

4.4.4. Effect of weld metal microstructure and anisotropic material property

Although mixed mode loading is believed as the primary cause of loss of directional stability by many researchers, microstructure changes in the weld metal also contribute to the crack directional instability. In the test specimens, initial crack plane was 5 mm from the weld nugget centre meaning that material properties are different for each side of the crack plane, i.e. weld nugget property on one side of the crack and TMAZ/HAZ on the other side.

Furthermore, alloy 2198-T8 has highly anisotropic microstructures [24-25]. According to Yates et al. [14], highly anisotropic microstructures can also lead to significant changes in crack orientation, but more often in a zigzag pattern maintaining the overall mode-I trajectory. Crack path deviation triggered by material property irregularity can be enhanced by the applied biaxial loads as demonstrated by the test results in Fig. 4b. Test measured crack growth route shows a zigzag path when a < 70 mm [18]. However, predicted crack deviation is in one direction. Crack turning angle is determined by the sign of K_{II}, which is function of applied stress and geometry but not the material property. It is worth noting that crack deviation was not observed in M(T) under uniaxial loading with weld perpendicular to the loading direction, but observed in the cruciform specimen under biaxial loads; this is due to the influence of K_{II} and T-stress.

4.4.5. Other influential factors

Welding-induced distortion was significant in magnitude [18]. In the tests initial distortion was corrected by applying clamping forces at the specimen's four loading ends. This will affect the initial stress condition in the specimen. The initial distortion was not completely illuminated by clamping. However, the initial out-of-plane deformation and clamping force induced initial stresses were not modelled. This could affect the accuracy in the predicted crack growth rates and trajectory. Test specimens involved two material rolling directions in relation to the welding and crack growth direction, showing that the material rolling direction affects the crack growth path. This is caused by material anisotropy [24-25], weld microstructure change, and residual stresses in both material directions. However, these effects are not modelled. Research also shows that crack location within weld, e.g. in the nugget centre or the HAZ, will also influence the crack growth rates considerably [26].

5. Summary and Conclusions

Finite element analysis was performed for a cruciform specimen containing weld joint and being subjected to biaxial cyclic loads. First, stress distribution and out-of-plane deformation are determined to assess the effect of secondary bending on fracture mechanics parameters. Second, influence of biaxial stress on crack growth behaviour is modelled, and fatigue crack growth life is predicted using calculated stress intensity factors and weld metal crack growth rates measured from M(T) specimens made of the same material and same welding process. Main conclusions are:

1. Mode-I stress intensity factor (SIF) decreases as the biaxial load ratio k increases. Comparing to the uniaxial load case ($k = 0$), reduction in SIF is 12% ($k = 1$) and 24% ($k = 2$).
2. For $k \leq 1$, no crack path deviation is predicted by the analysis; models show very small deviation when a crack is longer than half of the panel width. For $k = 2$, small deviation is predicted. The model solution is in agreement with the fracture mechanics theory based on the mode II SIF and elastic T stress.
3. Test observed crack turning is larger than model prediction. This could be due to a few complex factors that are not considered in the present FE model, such as weld metal microstructure, anisotropic material properties, and residual stress in the weld longitudinal direction.

Acknowledgement

The authors are grateful for the financial support from the European Union through its Sixth Framework Programme under the “cost effective integral metallic structures” project. They also thank Drs. Richter-Trummer and Dos Santos at Helmholtz-Zentrum Geesthacht Germany for providing test data. The modelling work was conducted at Cranfield University.

References

1. Bussu G, Irving PE. The role of residual stress and heat affected zone properties on fatigue crack propagation in friction stir welded 2024-T351 aluminium joints, Int J Fatigue, 25(2003): 77-88.
2. Pouget G, Reynolds AP. Residual stress and microstructure effects on fatigue crack growth in AA2025 friction stir welds, Int J Fatigue, 30(2008): 463-472.
3. Glinka G. Effect of residual stresses on fatigue crack growth in steel weldments under constant and variable amplitude load. In: Fract. Mech., ASTM STP 677, American Society for Testing and Materials, 1979, pp. 198-214.
4. Beghini M, Bertini L, Vitale E. Fatigue crack growth in residual stress fields: experimental results and modelling. Fatigue Fract Engng Mater Struct 1994; 17: 1433-1444.
5. Ghidini T, Dalle Donne C. Fatigue crack propagation assessment based on residual stresses obtained through cut-compliance technique, Fatigue & Fracture of Eng Mater & Struct, 30(2006): 214-222.
6. Fratini L, Pasta S, Reynolds AP, Fatigue crack growth in 2024-T351 friction stir welded joints: longitudinal residual stress and microstructural effects. Int J Fatigue 2009; 31: 495-500.
7. Servetti G, Zhang X. Predicting fatigue crack growth rate in a welded butt joint: the role of effective R ratio in accounting for residual stress effect. Eng Fract Mech 76 (2009) 1589-1602.
8. Cotterell B. International J of Fracture Mechanics, 2 (1966): 526-533.

9. Leevers PS, Radon JC, Culver LE. J of mechanics and Physics of Solids, 24 (1976), 381-395.
10. Liu AF, Allison JE, Dittmer DF, Yamane JR. Effect of biaxial stresses on crack growth, Fracture Mechanics, ASTM STP 677, CW Smith ed., ASTM, 1979, pp. 5-22.
11. Brown MW, Miller KJ. Mode I fatigue crack growth under biaxial stress at room and elevated temperature, ASTM STP 853, 1985, 135-152.
12. Eftis J, Jones D L, Liebowitz H. Load biaxiality and fracture: synthesis and summary. Engineering Fracture Mechanics, 36 (1990): 537-574.
13. Llopart L, et al. Investigation of fatigue crack growth and crack turning on integral stiffened structures under mode I loading, Engineering Fracture mechanics, 73 (2006):2139-2152.
14. Yates JR, et al. Crack paths under mixed mode loading, Engineering Fracture mechanics, 75 (2008): 319-330.
15. Pook LP, Five decades of crack path research, Engineering Fracture mechanics, 77 (2010):1619-1630.
16. Huang W-L, Zhu W, Zhao J-P. Effect of lateral load on fatigue growth rate of surface cracks in welded joints, Int J Pres Ves & Piping, 69 (1996): 59-64.
17. Erdogan F, Sih G. On the crack extension in plates under plane loading and transverse shear, J of Basic Engineering, 85(1963): 519-527.
18. Richter-Trummer V, Dos Santos J. Biaxial fatigue crack propagation testing, Technical Report, 2010, Helmholtz-Zentrum Geesthacht, Institute of Materials Research, Geesthacht, Germany.
19. Anonymous. ABAQUS/Standard User's Manual, V6.5. Hibbitt, Karlsson & Sorensen, 2005
20. Ma Y-E, Irving PE, Zhang X, Servetti G, Effects of residual stresses on fatigue crack propagation in friction stir welded 2198-T8 and 2195-T8 Al-Li alloy joints, Proc 12th Int Conf. in Fracture (ICF12), July 2009, Ottawa.
21. Zhang H. Numerical Modelling of Crack Propagation in a Friction Stir Welded Cruciform Specimen. MSc Thesis, Cranfield University, 2009.
22. Cotterell B, Rice JR. Slightly curved or kinked cracks, Int J of Fracture, 16 (1980): 155-169
23. Pook, LP. Crack Paths. WIT Press, Southampton. 2002 (Eq. 4.4).
24. Cavaliere P, De Santisa A, Panellaa F, Squillaceet A. Effect of anisotropy on fatigue properties of 2198 Al–Li plates joined by friction stir welding, Engineering Failure Analysis, 2008.
25. Cavaliere P, Cabibboc M, Panellaa F, Squillace A. 2198 Al–Li plates joined by friction stir welding: mechanical and microstructural behavior, Materials and Design 30 (2009): 3622–3631
26. Pacchione M, Werner S, Ohrloff N. Design principles for damage tolerant butt weld joints for application in the pressurized fuselage, Proceedings 24th Symposium of International Committee on Aeronautical Fatigue (ICAF 2007), Naples, May 16-18, 2007